Supporting Information

Hazak et al. 10.1073/pnas.1413918111

SI Materials and Methods

Plant Material, Growth Conditions, and DNA Constructs. *Arabidopsis thaliana* ecotype *Columbia-0* (*Col-0*) was used in all experiments. *DII-VENUS* seeds were obtained from the Nottingham *Arabidopsis* Stock Centre. The following lines have previously been described: $DR5_{rev}$*::GFP* (1), *DII-VENUS* (2), *DR5::β-Glucoronidase* (*GUS*) (3), *pICR1>>GFP-ICR1* (4), and *35S::GFP-ICR1* (5). *pCMI2>>GFP-ICR1* and *pICR1>>ICR1-m-Cherry* lines were created with the LhG4 transcription/transactivation system (4, 6). A fragment of 2,050 bp upstream to the ATG initiation codon of *CMI2* (*At4g54490*) was amplified by PCR with Phusion DNA polymerase (Thermo Scientific) from genomic DNA. The amplified fragment was cloned into *pJET* (Thermo Scientific) to create *pSY1543*. *pSY1543* was digested with SalI and KpnI and subcloned into *pBj36* (4, 6) to make *pS1544*. *pS1544* was digested with NotI to isolate a fragment containing the *pCMI2* and LhG4 and subcloned into the *pART* (6, 7) plant binary vector to make *pSY1545*. *Agrobacterium tumefaciens* (*GV3101*/*pMP90*) containing *pSY1545* was used to transform *Arabidopsis Col-0* plants using the floral dip method (8). The *pCMI2>>GFP-ICR1* plants were crossed into *DR5::GUS*. Seedlings were grown vertically on 0.5× Murashige and Skoog (MS; Duchefa) medium supplemented with 1% sucrose under long-day (16-h light/8-h dark) conditions at 22 °C. Light intensity was 100 μE m^{-2} s^{-1}. *pICR1>>ICR1-mCherry* plants were created by crosses between *pICR1::LhG4* and *pop-ICR1-mCherry*. To create *pop-ICR1-mCherry*, a PCR fragment of ICR1 with SalI and KpnI sites was cloned into *pJET1.2*; then, an mCherry PCR fragment was fused to ICR1 at the KpnI restriction site. The *ICR1-mCherry* fragment from *pJET1.2* was subcloned using SalI and KpnI restriction sites of the *10 OP TATA*/*BJ36* vector.

Plant Treatments.

Root tip excisions and chemical treatments. Excisions were performed as previously described (9). For treatments, immediately after excision, seedlings were transferred to 0.5× MS plates supplemented with 1% sucrose and one of the following inhibitors: 50 μM MG132, 10 μM NPA, 5 μM auxinole, or 10 μM CHX. Stock solutions were prepared as follows: NAA and IAA (Sigma) in ethanol, 2,4-D (Sigma) in 0.1 M KOH in ethanol, and NPA (Duchefa), MG132 (Calbiochem), CHX (Sigma), and auxinole (gift from Ken-ichiro Hayashi, Okayama University of Science, Okayama, Japan) (10, 11) in DMSO. Dilution into medium was at indicated concentrations. For the 2,4-D and NAA treatments, 5-d-old vertically grown seedlings were transferred to plates containing 1 μM 2,4-D or 0.5 μM NAA. GUS staining was carried out as previously described (12).

Gravitropic response. Seedlings were germinated vertically for 5 d on 0.5× MS 1% sucrose medium. Plates were tilted 90° for indicated time points (0, 10, 20, 30, 40, and 50 min). For imaging, seedlings were moved to previously prepared slides with propidium iodide and imaged immediately. Fluorescent intensity was quantified in ∼30 seedlings for each time point.

Tissure clearing. Tissue clearing for Nomarsky differential interference contrast optics was carried out as previously described (4).

Quantification of the auxin response using $DR5_{rev}$::GFP and pICR1>>GFP-ICR1 after 0.5 μM NAA treatment. Seedlings were grown under long-day conditions (16-h light/8-h dark) in vertically oriented 0.5× MS 1% sucrose agar plates. After 5 d, the seedlings were transferred to new 0.5× MS 1% sucrose plates supplemented with 0.5 μM NAA and grown under long-day conditions for 3 or 24 h. Imaging was carried out on 10 seedlings from each line. Fluorescence intensity in designated regions was measured with Fiji (Image J). *P* values were calculated with Wilcoxon rank test.

Quantification of GFP-ICR1 during LR development. Analysis was carried out on *pICR1>>GFP-ICR1* seedlings grown on vertically oriented 0.5× MS 1% sucrose agar plates for 10 d. Fluorescence quantification was carried out on 10 LRI/LR for each developmental stage (stages III and IV, stage VI to emergence, and 200-μm-long LRs). Fluorescence intensity was measured in equal areas in the stele (or vascular precursors) and QC cells (or two central cells of the outer layer 2) (Fig. S4*C*). The fluorescence intensity ratio between QC and stele was calculated for each sample to overcome variability in fluorescence intensity between different LRs. *P* values were calculated with the Wilcoxon rank test.

Quantification of DII-VENUS after root sectioning. Five-day-old *DII-VENUS* seedlings were used for root excisions. Root tips were either imaged immediately after sectioning (5 min) or transferred to 0.5× MS 1% sucrose plates and placed in a growth chamber for 30 min, 60 min, or 24 h before imaging. Fluorescence intensity of single nuclei was measured using Fiji (Image J). Analysis was carried out on images taken from four sectioned roots for each time point. In each image, fluorescence was measured in 20 nuclei in the cell layers close to the site of excision (area 1) and 20 nuclei in the stele cells 80 μm above the site of excision (area 2). The ratios between area 1 and area 2 were used to determine the percentage of DII-VENUS signal decay. Data were analyzed by curve fitting: ratio = $1.123 - 0.126 \times \log(\text{time})$.

Immunolocalization. Five-day-old *Col-0* seedlings were fixed with 100 mM Pipes (pH 6.89), 5 mM EGTA, 5 mM $MgSO_4 \times 7H_2O$ (buffer A), and 1% Triton X-100 for 5 min and in turn, buffer A and 8% (vol/vol) paraformaldehyde. Fixation was carried out at room temperature in the dark. Samples were then rinsed three times in buffer A and treated with the following enzyme mixture: 2% (wt/vol) cellulase onzuka R-10 (Yakult) and 1% pectinase containing protease inhibitor mixture (Sigma) and 20 μM PMSF for 10 min. After washing in buffer A for 30 min, the samples were gently squashed on coverslips coated with poly-L-lysine (1 mg/mL; Sigma). Then, the tissues were retreated for 10 min with enzyme mixture [2% (wt/vol) cellulase onzuka R-10, 1.5% (wt/vol) pectinase] with protease inhibitors. This step was followed by a rinse in PBS with 1% Triton X-100 for 30 min and then, incubation in PBS containing 1% BSA for 20 min. To reduce aldehyde-induced autofluorescence, samples were treated for 5 min with 10 mg/mL sodium borohydride in PBS and then washed in PBS for 20 min. For immunofluorescence detection of ICR1, specimens were incubated overnight at room temperature with primary mouse anti-ICR1 polyclonal antibodies at a dilution of 1:100. Samples were then washed in PBS and incubated with anti-mouse secondary antibodies conjugated to Alexa 555 (Molecular Probes) diluted 1:100 for 1 h at room temperature. Mounting was done in 50% (vol/vol) glycerol/water.

Microscopy. Low-resolution imaging was performed with an SV-11 stereomicroscope (Zeiss). Nomarsky differential interference contrast optics was performed with a Axioplan 2 Imaging microscope (Zeiss). Confocal imaging was performed with either a TCS-SL confocal laser-scanning microscope (Leica) with a 20× multiimmersion objective and an N.A. of 0.7 or a Zeiss LSM 780-NLO combined laser-scanning confocal microscope and multiphoton microscope (Zeiss) using a 20× dry objective and an N.A. of 0.8. GFP was visualized by excitation with an argon laser at 488 nm with a 500-nm beam splitter, and the spectral detector

was set between 505 and 530 nm. Propidium iodide was visualized by excitation with an argon laser set to 514 nm, a 456/514-nm double dichroic beam splitter, and a spectral detector set between 530 and 560 nm. Image analysis was performed with Fiji (Image J), Leica TCS, Zeiss Zen 10, and Adobe Photoshop 6.

Primers Used in This Study. For cloning primers, the *pCMI2* was amplified using the following oligonucleotide primer pair: forward, SY2234P: AAGTCGACACTCTATGATTGCGTCAATCATAA and reverse, SY2235P: TAGGTACCTACAAAAGAAGAAAAAGTAAAACAGTTTG.

For *pop-ICR1-mCherry* cloning, we used ICR1 SalI F: TAGTCGACATGCCAAGACCAAGAGTTTCAGA; ICR1 KpnI R: TAGGTACCCTTTTGCCCTTTCTTCCTCCACAAC; mCherry KpnI R: TAGGTACCTTACTTGTACAGCTCGTCCATGC; and mCherry KpnI F: TAGGTACCTTACTTGTACAGCTCGTCCATGC.

Mathematical Modeling. We modeled an $m \times n$ array of cells representing a root tip. In each cell indexed (i,j), we model the auxin concentration $(AUX_{i,j})$ and the level of ICR1 found adjacent to the cell's four-membrane planes ($\mathrm{ICR1}_{i,j}^{Up}$, $\mathrm{ICR1}_{i,j}^{Right}$, $\mathrm{ICR1}_{i,j}^{Down}$, and $\mathrm{ICR1}_{i,j}^{Left}$).

The rate of change of auxin concentration in cell (i,j) for $1 < i < m$ and $1 < j < n$ is given by

$$\begin{aligned}\frac{d(AUX_{i,j})}{dt} = &-AuxInact \times AUX_{i,j} \\ &+ D\left(AUX_{i-1,j} + AUX_{i+1,j} + AUX_{i,j+1}AUX_{i,j-1} - 4\right. \\ &\left.\times AUX_{ij}\right) + K\left(AUX_{i-1,j} \times \mathrm{ICR1}_{i-1,j}^{Down} + AUX_{i+1,j}\right. \\ &\times \mathrm{ICR1}_{i+1,j}^{Up} + AUX_{i,j+1} \times \mathrm{ICR1}_{i,j+1}^{Left} + AUX_{i,j-1} \\ &\left.\times \mathrm{ICR1}_{i,j-1}^{Right}\right) - K \times AUX_{i,j} \\ &\times \left(\mathrm{ICR1}_{i,j}^{Down} + \mathrm{ICR1}_{i,j}^{Up} + \mathrm{ICR1}_{i,j}^{Left} + \mathrm{ICR1}_{i,j}^{Right}\right).\end{aligned}$$

Our equations are similar to the equations presented in refs. 13 and 14 for PIN-regulated auxin transport. The auxin inactivation rate and ICR1-independent transport rate are proportional to the auxin concentration in the cell, and the proportion constants are *AuxInact* and *D*, respectively. ICR1-dependent auxin transport is proportional to the product of the auxin concentration in the cell and the level of ICR1-dependent auxin efflux through the appropriate neighboring cell membranes. The proportion constant determining the rate of transport is denoted by *K*. Cells for which $i \in \{1,m\}$ *and* $j \in \{1,n\}$ (cells located at the corners of the matrix) follow similar dynamics, with ICR1-dependent and -independent transport occurring only from the possible neighboring cells. Cells $(1,j)$ (the uppermost row of cells), in which $1 < j < m$ have an additional term of auxin influx given by *AuxInf*.

The rate of change of ICR1-dependent transport through the h cell membrane, where $h \in \{Up, Down, Right, Left\}$ in cell (i,j) for $1 < i < m$ and $1 < j < n$, is given by

$$\frac{d\left(\mathrm{ICR1}_{i,j}^{h}\right)}{dt} = \mathrm{ICR1}Syn \times \frac{\left(\frac{AUX_{i_h,j_h}\left(D + K \times \mathrm{ICR1}_{i_h,j_h}^{h}\right)}{q_1}\right)^{c_1}}{1 + \left(\frac{AUX_{i_h,j_h}\left(D + K \times \mathrm{ICR1}_{i_h,j_h}^{h}\right)}{q_2}\right)^{c_1}}$$

$$-\mathrm{ICR1}Deg \times \left(1 + \left(\frac{AUX_{i_h,j_h}\left(D + K \times \mathrm{ICR1}_{i_h,j_h}^{h}\right)}{q_3}\right)^{c_1}\right) \times \mathrm{ICR1}_{i,j}^{h},$$

where (i_h,j_h) are the appropriate indices for the cell adjacent to cell (i,j) from a direction opposite to h [e.g., $\mathrm{ICR1}_{i,j}^{Down}$ will be affected by the auxin flow from the cell above it $((i_h,j_h) = (i-1,j))$, which is determined by the product of the auxin levels in that cell $(AUX_{i-1,j})$ and the ICR1-mediated transport in the bottom cell membrane plane $(\mathrm{ICR1}_{i-1,j}^{Down})$]. ICR1 synthesis and degradation are modeled using hill functions with the constants ICR1*Syn* and ICR1*Deg*. The auxin influx thresholds for ICR1 synthesis, saturation, and degradation are given by q_1, q_2, and q_3, respectively.

The initial auxin concentration was set to a uniform distribution, with every cell having a unit concentration of auxin. All other parameters were normalized to the unit auxin concentration. The passive auxin transport rate (D) was set to 0.08 for all cells; the auxin influx $(AuxInf)$ was set to 0.5 for each cell of the upper row, excluding the two outermost cells. These values were chosen according to observed ranges (13). Auxin influx and degradation rates were chosen to balance auxin influx, namely $Inact = (n - 2/m \times n) \times AuxInf$. All other ICR1-dependent parameters (K, ICR1*Syn*, ICR1*Deg*, q_1, q_2, q_3, and c_1) were chosen to fit the observations.

The parameter values and interpretations are given in Table S2.

1. Reinhardt D, et al. (2003) Regulation of phyllotaxis by polar auxin transport. *Nature* 426(6964):255–260.
2. Brunoud G, et al. (2012) A novel sensor to map auxin response and distribution at high spatio-temporal resolution. *Nature* 482(7383):103–106.
3. Ulmasov T, Murfett J, Hagen G, Guilfoyle TJ (1997) Aux/IAA proteins repress expression of reporter genes containing natural and highly active synthetic auxin response elements. *Plant Cell* 9(11):1963–1971.
4. Hazak O, et al. (2010) A rho scaffold integrates the secretory system with feedback mechanisms in regulation of auxin distribution. *PLoS Biol* 8(1):e1000282.
5. Lavy M, et al. (2007) A Novel ROP/RAC effector links cell polarity, root-meristem maintenance, and vesicle trafficking. *Curr Biol* 17(11):947–952.
6. Moore I, Gälweiler L, Grosskopf D, Schell J, Palme K (1998) A transcription activation system for regulated gene expression in transgenic plants. *Proc Natl Acad Sci USA* 95(1):376–381.
7. Eshed Y, Baum SF, Perea JV, Bowman JL (2001) Establishment of polarity in lateral organs of plants. *Curr Biol* 11(16):1251–1260.
8. Clough SJ, Bent AF (1998) Floral dip: A simplified method for Agrobacterium-mediated transformation of Arabidopsis thaliana. *Plant J* 16(6):735–743.
9. Sena G, Wang X, Liu HY, Hofhuis H, Birnbaum KD (2009) Organ regeneration does not require a functional stem cell niche in plants. *Nature* 457(7233):1150–1153.
10. Hayashi K, et al. (2012) Rational design of an auxin antagonist of the SCF(TIR1) auxin receptor complex. *ACS Chem Biol* 7(3):590–598.
11. Hayashi K, et al. (2008) Small-molecule agonists and antagonists of F-box protein-substrate interactions in auxin perception and signaling. *Proc Natl Acad Sci USA* 105(14):5632–5637.
12. Weigel D, Glazebrook J (2002) *Arabidopsis: A Laboratory Manual* (Cold Spring Harbor Lab Press, Plainview, NY).
13. Mironova VV, et al. (2010) A plausible mechanism for auxin patterning along the developing root. *BMC Syst Biol* 4:98.
14. Mironova VV, et al. (2012) Combined in silico/in vivo analysis of mechanisms providing for root apical meristem self-organization and maintenance. *Ann Bot (Lond)* 110(2): 349–360.

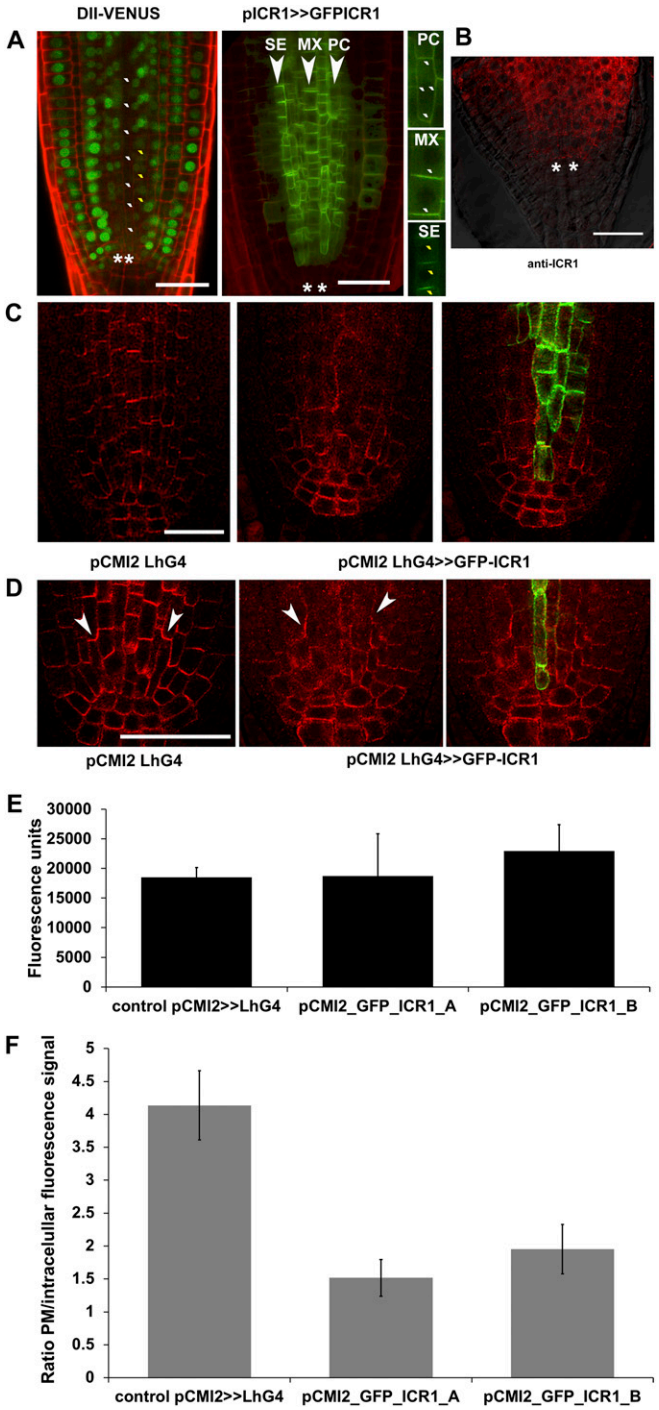

Fig. S1. (*A*) Expression of (*Left*) the auxin sensor DII-VENUS in the root tip area and (*Center* and *Right*) GFP-ICR1. Note the decreased DII-VENUS abundance in the nuclei of provascular tissue metaxylem (MX; white marks) and the protophloem sieve element (SE; yellow marks) and the absence of DII-VENUS signal in the quiescent center (QC) cells (white asterisks). *Right* shows enlargements of different cell files. Note that, in the cells with slightly higher auxin levels, GFP-ICR1 shows polarized (apical–basal and not lateral) localization. (*B*) Immunolocalization of ICR1 in the root tips decorated with anti-ICR1 antibodies. Note the absence of signal in the QC (asterisks). (*C*) Immunolocalization of PIN4 in control *pCMI2::LhG4* and *pCMI2>>GFP-ICR1* line A root tips. (*D*) Immunolocalization of PIN4 in control *pCMI2::LhG4* and *pCMI2>>GFP-ICR1* line B plants. (*Right*) Overlay of PIN4 (red) and GFP-ICR1 (green). (*E* and *F*) Quantification of PIN4 levels in membranes of *pCMI2>>LhG4* and *pCMI2>>GFP-ICR1* root tips. (*E*) Bars represent total PIN4 fluorescence in the measured area. (*F*) Bars represent a ratio of the plasma membrane fluorescence to intracellular fluorescence. Error bars correspond to SE (Table S1). The plasma membrane (PM) levels of PIN4 were measured by Image J in multiple roots at the same location in the meristematic zone. The total fluorescence in *pCMI2>>GFP-ICR1* was higher than in the control *pCMI2>>LhG4* roots because of higher intracellular background fluorescence. To distinguish between the intensity of fluorescent signal at the PM and intracellular signal, the intensity of membrane-localized PIN4 was extracted as the increase of the signal from background fluorescence in a measured location. (Scale bars: 50 μm.)

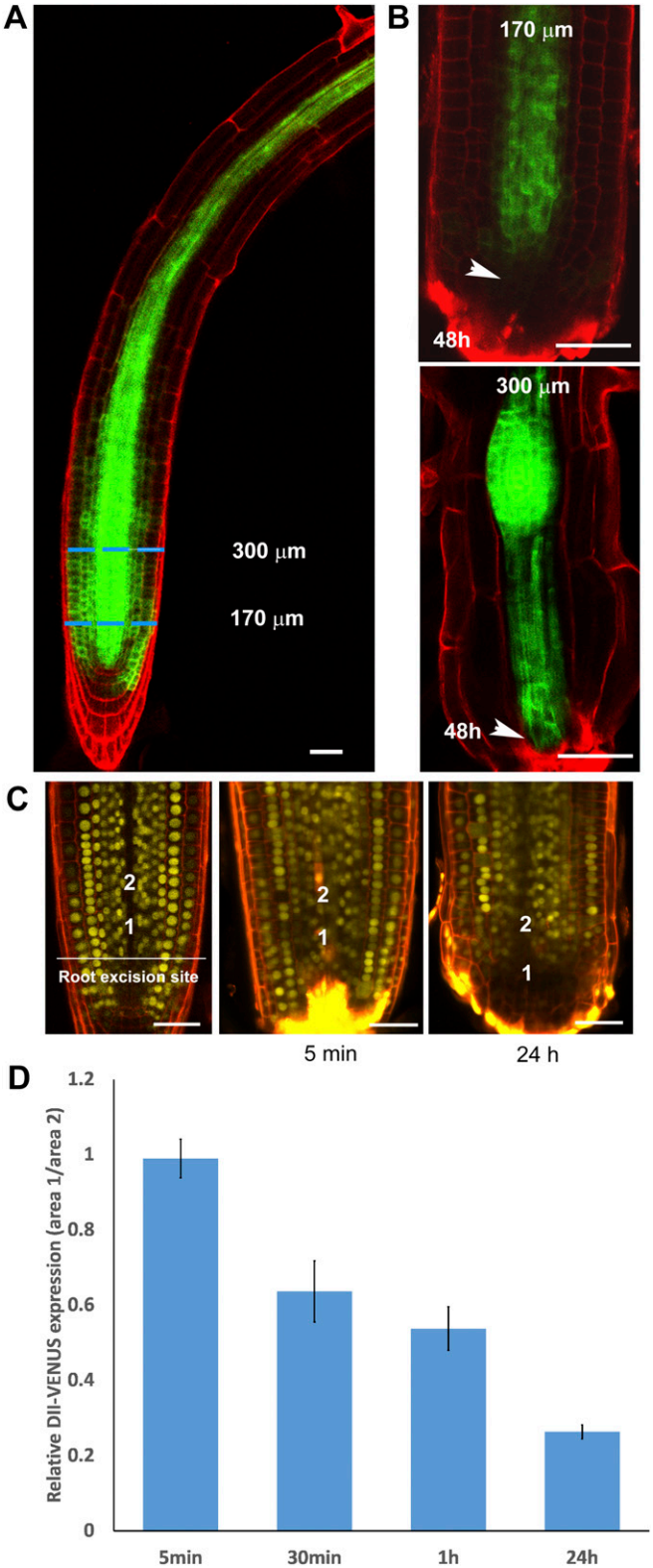

Fig. S2. GFP-ICR1 and DII-VENUS destabilization during root meristem regeneration. (*A*) A root expressing GFP-ICR1. The dashed blue lines denote sectioning at 170 and 300 μm from the tip. (*B*) Forty-eight hours after sectioning, GFP-ICR1 was absent from the regenerating meristem of the root sectioned 170 μm from the tip and present in the root sectioned 300 μm from the tip, in which the meristem did not regenerate (arrowheads). Note the accumulation of GFP-ICR1 in the developing LR primordium. Propidium iodide-labeled cell walls (red) and GFP-ICR1 (green) are shown. (Scale bars: 50 μm.) (*C* and *D*) Quantification of DII-VENUS decay during root regeneration. (*C*) Representative images highlighting the excision site (white line). Fluorescence quantification was carried out on 20 nuclei from the cell layers close to the site of excision (1) and 80 μm above the site of excision (2). (*D*) The ratios between areas 1 and 2 were used to determine the percentage of DII-VENUS signal decay. The bars represent SE.

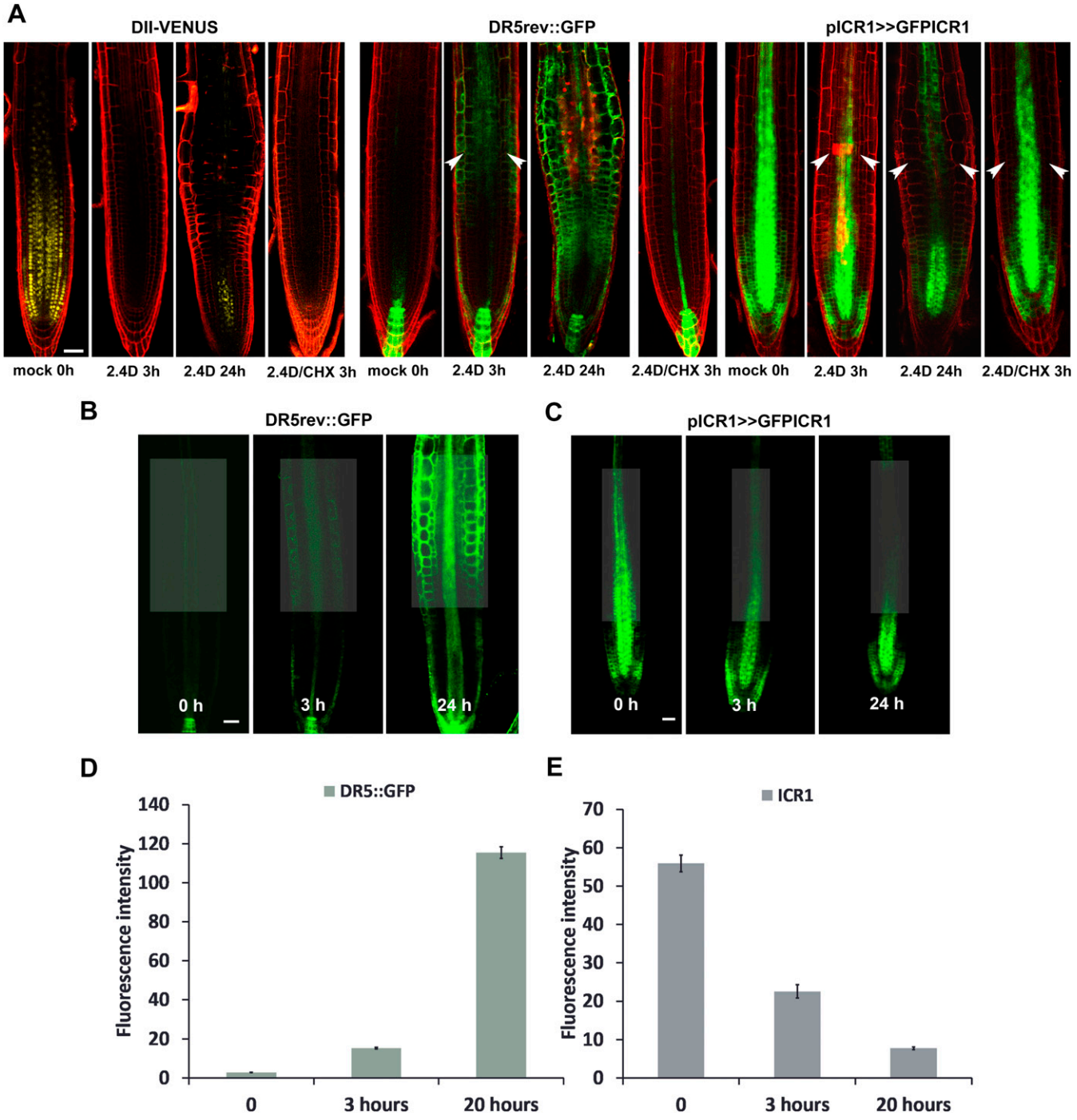

Fig. S3. ICR1 destabilization after exogenous auxin treatments. (*A*) DII-VENUS, $DR5_{rev}$::GFP, and GFP-ICR1 levels in seedlings treated with 1 μM 2,4-D with or without 20 μM CHX and imaged after 3 or 24 h. Arrowheads denote regions where the GFP-ICR1 signal was reduced at about 500 μm from the tip. (Scale bars: 50 μm.) (*B–E*) Concomitant up-regulation and down-regulation of $DR5_{rev}$::GFP and GFP-ICR1 500 μm from the root tip after treatments with NAA. Levels of (*B*) $DR5_{rev}$::GFP and (*C*) GFP-ICR1 in roots before or 3 or 24 h after transfer to 0.5 μM NAA-supplemented medium. Gray rectangles highlight areas that were used for signal quantifications and are shown in *D* and *E*. Quantification of (*D*) $DR5_{rev}$::GFP (DR5::GFP) and (*E*) GFP-ICR1 (ICR1) levels in regions corresponding to the highlighted areas in *B* and *C*. Signal quantification was carried out on 10 roots. Bars are SE ($P \leq 0.0022$ Wilcoxon rank test).

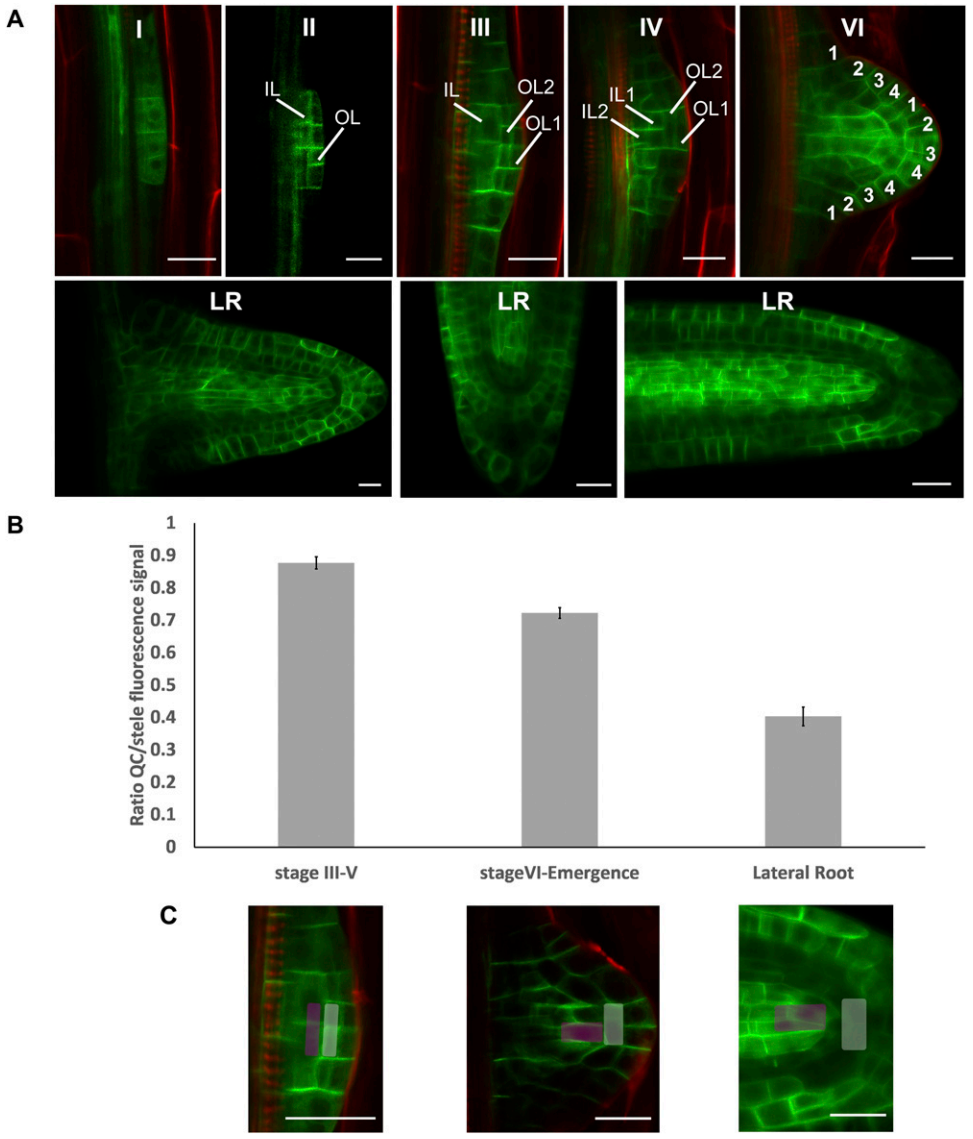

Fig. S4. Levels and localization of GFP-ICR1 during LR development. (*A*) GFP-ICR1 is detected in stage I of LR development. Note the absence of the GFP-ICR1 signal in the QC 150- to 300-μm-long LRs. Roman numerals correspond to the developmental stages of the LRI. Numbers on the epidermis correspond to the developmental stages of the LR. All labeling is according to the work by Malamy and Benfey (1). IL, inner layer; OL, outer layer. (*B*) Quantification of the reduction in GFP-ICR1 signal intensity in the QC during LR development. To avoid errors caused by differences in signal intensities between individual LRs, the results are presented as change in the ratio of the signal between the QC and stele in each LR. Analysis was carried out on 10 LRs for each developmental stage. Error bars are SE ($P \leq 0.002$ Wilcoxon rank test). (*C*) Representative images of LRs used for quantifications. Quantified regions are highlighted by purple and white rectangles.

1. Malamy JE, Benfey PN (1997) Organization and cell differentiation in lateral roots of Arabidopsis thaliana. *Development* 124(1):33–44.

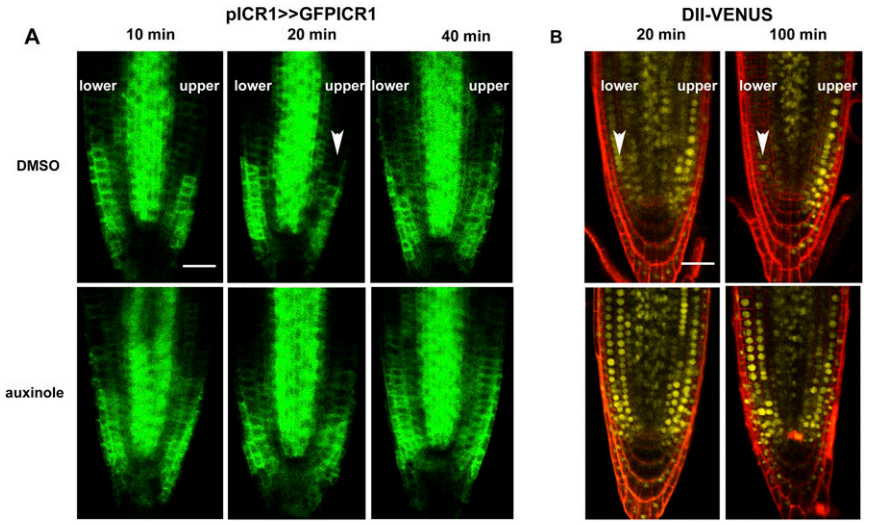

Fig. S5. ICR1 destabilization during root gravitropic response requires auxin-induced gene expression. The $SCF^{(TIR1/AFB)}$ inhibitor auxinole inhibited reduction of (*A*) GFP-ICR1 levels in the upper side and (*B*) DII-VENUS in the lower side of 90° tilted roots. Arrowheads highlight the sites of GFP-ICR1 and DII-VENUS destabilization. (Scale bars: 50 μm.)

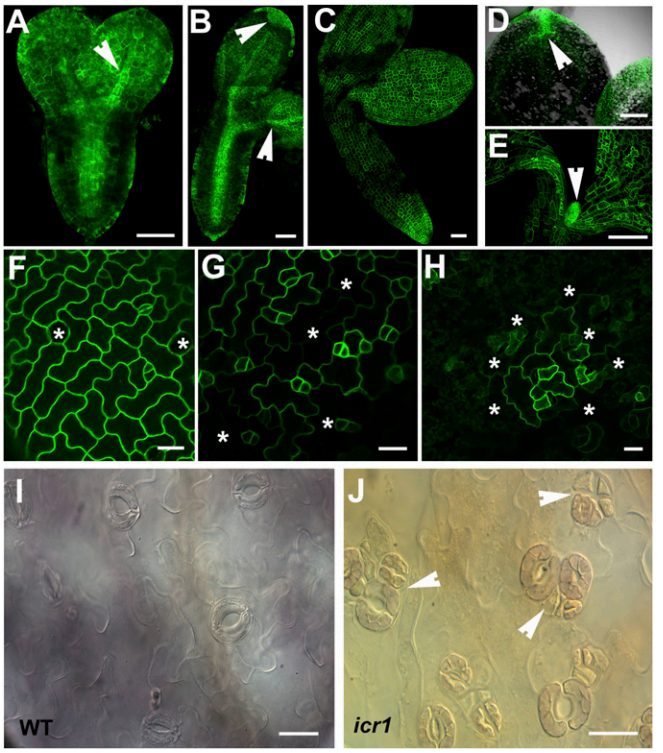

Fig. S6. GFP-ICR1 expression pattern in cotyledon and leaves. (*A*–*H*) pICR1>>GFPICR1 expression pattern embryos, cotyledons, and leaves. (*A*) Torpedo-stage embryo. The arrowhead denotes the provascular tissue. (*B* and *C*) Mature embryos. Arrowheads in *B* denote higher GFP-ICR1 levels in the cotyledon tip (upper cotyledon) and the provascular tissue (lower cotyledon). (*D*) A 4-d-old seedling. The arrowhead denotes higher GFP-ICR1 expression at the cotyledon tip and subtending provascular tissue. (*E*) High GFP-ICR1 expression in leaf primordium (arrowhead). (*F*) A 2-d-old seedling cotyledon epidermis. No expression was detected in mature stomata guard cells (asterisks). (*G*) A 5-d-old cotyledon epidermis. Note the higher expression levels of GFP-ICR1 in developing stomata lineage cells and absence in mature pavement and stomata guard cells (asterisks). (*H*) Epidermis of 6-wk-old plant leaf number 10. The asterisks denote mature pavement and stomata guard cells. (*I* and *J*) Nomarsky differential interference contrast images of 5-d-old seedlings. (*I*) WT *Col-0*. (*J*) *icr1*. Note the appearance of the stomata clusters in *icr1* (arrowheads). Images in *F*–*J* are of the adaxial epidermis. (Scale bars: *A*–*C* and *F*–*J*, 25 μm; *D* and *E*, 150 μm.)

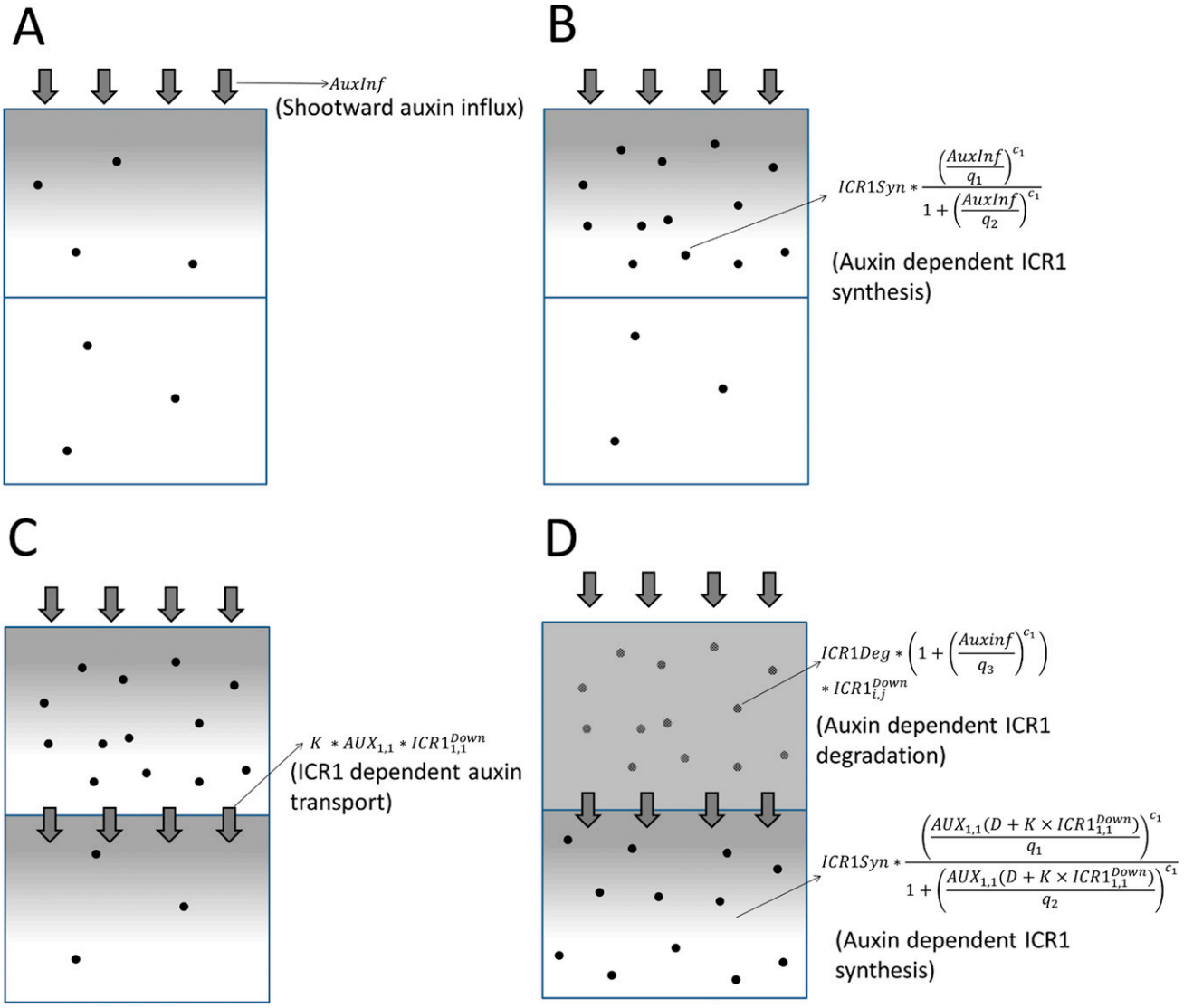

Fig. S7. Graphic explanation of the mathematical model. The dynamics of auxin concentration are illustrated for cells (*Upper*) (1,1) and (*Lower*) (1,2). Auxin concentrations are represented by the color gradient; darker areas represent higher auxin concentrations. ICR1 is represented by black circles. For simplicity, the direction of auxin flow is represented only in one dimension. Parts of the process described in the equations given in the text and *SI Materials and Methods* are illustrated. (*A*) Auxin levels rise in cell (1,1) because of auxin influx from upper cells. (*B*) ICR1 is synthesized because of the moderate auxin levels in cell (1,1). (*C*) Auxin begins to flow from cell (1,1) to cell (1,2) because of the increase in ICR1 and auxin flow in cell (1,1). (*D*) ICR1 is degraded in cell (1,1) because of high auxin levels, whereas ICR1 is synthesized in cell (1,2) because of moderate auxin levels.

Table S1. Quantification of PIN4 levels in *pCMI2>>LhG4* and *pCMI2>>GFP-ICR1* roots

	Total fluorescence	SE total fluorescence	Ratio PM/intracellular fluorescence signal	SE ratio PM/intracellular fluorescence signal
Control *pCMI2>>LhG4* (n = 7)	18,482.77229	1,689.073949	4.135894283	0.524940881
pCMI2>>GFP-ICR1-A (*n* = 3)	18,724.72733	7,125.194709	1.517253465	0.278969595
pCMI2>>GFP-ICR1-B (*n* = 7)	22,956.332	4,445.876208	1.951623823	0.375279473

Quantification of immunostaining signals. The plasma membrane (PM) and intracellular fluorescence signals (arbitrary units) of PIN4 in control *pLCMI2>>LhG4* and two *pCMI2>>GFP-ICR1* lines are given. The data in the table correspond to Fig. S1 *E* and *F*.

Table S2. Parameters of the mathematical model (Fig. 6)

Parameter	Meaning	Value
D	Passive auxin transport rate	0.08
AuxInf	Auxin influx rate	0.5
AuxInact	Auxin inactivation rate	$\frac{5}{m*n} * AuxInf$
K	Active auxin transport rate	5 (0 for Fig. 6*B*)
ICR1Syn	ICR1 synthesis rate	0.1
ICR1Deg	ICR1 degradation rate	0.17 (10^{-9} for Fig. 6*D*)
q_1	Auxin influx threshold for ICR1 synthesis	1.21
q_2	Auxin influx threshold for ICR1 saturation	1.5
q_3	Auxin influx threshold for ICR1 degradation	1.3
c_1	Hill function coefficient	2
m, *n*	No. of rows and columns	14, 7

Parameters used in the mathematical model shown in Fig. 6.